

Toward a Deterministic Model of Planetary Formation V.

Accumulation Near the Ice Line

S. Ida

Tokyo Institute of Technology, Ookayama, Meguro-ku, Tokyo 152-8551, Japan

`ida@geo.titech.ac.jp`

and

D. N. C. Lin

UCO/Lick Observatory, University of California, Santa Cruz, CA 95064

Kavli Institute of Astronomy & Astrophysics, Peking University, Beijing, China

`lin@ucolick.org`

ABSTRACT

We address two outstanding issues in the sequential accretion scenario for gas giant planet formation, the retention of dust grains in the presence of gas drag and that of cores despite type I migration. The efficiency of these processes is determined by the disk structure. Theoretical models suggest that planets form in protostellar disk regions with an inactive neutral “dead zone” near the mid plane, sandwiched together by partially ionized surface layers where magnetorotational instability is active. Due to a transition in the abundance of dust grains, the active layer’s thickness decreases abruptly near the ice line. Over a range of modest accretion rates ($\sim 10^{-9} - 10^{-8} M_{\odot} \text{ yr}^{-1}$), the change in the angular momentum transfer rate leads to local surface density and pressure distribution maxima near the ice line. The azimuthal velocity becomes super-Keplerian and the grains accumulate in this transition zone. This barrier locally retains protoplanetary cores and enhances the heavy element surface density to the critical value needed to initiate efficient gas accretion. It leads to a preferred location and epoch of gas giant formation. We simulate and reproduce the observed frequency and mass-period distribution of gas giants around solar type stars without having to greatly reduce the type I migration strength. The mass function of the short-period planets can be utilized to calibrate the efficiency of type I migration and to extrapolate the fraction of stars with habitable terrestrial planets.

Subject headings: planetary systems: formation – solar system: formation – stars: statics

1. Introduction

In the previous papers of this series (Ida & Lin 2004a,b, 2005, 2008, hereafter Papers I, II, III, and IV), we constructed a numerical scheme to simulate the anticipated mass and semimajor axis ($M_p - a$) distribution of planets based on a comprehensive treatment of the sequential planet formation scenario. In the scheme, we first generate a set of protoplanetary disk models with various surface densities and depletion timescales, on the basis of radio observations. For each disk, we randomly select semimajor axes of the protoplanetary seeds and integrate the growth of the protoplanets due to planetesimal accretion, assuming that planetesimals have been already formed from dust grains in the disks. If their masses become large enough, gas accretion onto the planets is also added. The planets’ orbits evolve through type I and type II migrations. We integrate growth and orbital evolution of planets independently, neglecting dynamical interactions between planets (see discussion in §3.3). For the integration, we use the semi-analytical prescriptions based on detailed numerical simulations. For details, see §3.3, Papers I and IV. In Paper I, we presented calculations for solar-type stars by neglecting the effect of type I migration on the basis that its efficiency is poorly determined. With the same assumptions, we simulated the $M_p - a$ distribution for stars with a range of metallicity ([Fe/H]) and mass (M_*) in Papers II and III, respectively.

As a consequence of their tidal interactions with surrounding disk gas, embedded embryos more massive than Mars migrate towards their host stars (Goldreich & Tremaine 1980; Ward 1986). In Paper IV, we have considered the influence of this type I migration on the planet formation process. Our results indicate that when this effect is fully taken into account, the icy cores have a tendency to migrate into their host stars before they acquire adequate mass to initiate efficient gas accretion. In order to preserve a sufficient fraction of cores which can subsequently evolve into the observed population of gas giants around solar type stars, we introduced a “type I migration reduction factor” C_1 . The magnitude of C_1 smaller than unity lengthens the actual magnitude of the type I migration timescale relative to that deduced from linear theories (Paper IV; also see the results in §3.3 and 3.4). With a range of small $C_1 \simeq 0.03 - 0.1$, we were able to simulate a planetary $M_p - a$ distribution which is qualitatively consistent with that observed by radial velocity survey.

While several suppression mechanisms for type I migration under various circumstances have been suggested (see references in Paper IV), the extremely small values of C_1 we have adopted in our previous models remains a challenge to our theoretical construct. In addition,

there remain some quantitative discrepancies between the results of our population synthesis and the observed a distribution of extrasolar planets. Around solar-type stars, existing data show an steep up turn in the frequency of detected planets with period around 1-4 yrs (corresponding to a in the range of 1-3 AU) (Cumming et al. 2008) whereas the predicted a distribution from our past models is essentially logarithmic (see the results in §3.3).

Another minor issue concerns with the availability of the building-block material for gas giants' cores. Current theory of gas giant formation requires a critical mass (M_{crit}) in excess of several earth masses in order for the onset of efficient gas accretion (e.g., Paper IV). But, the growth of embryos is limited by an isolation mass M_{iso} . For the minimum mass solar nebula (MMSN) model, the surface density distribution of the solid material ($\Sigma_d \propto a^{-3/2}$) implies M_{iso} is an increasing function of the semimajor axis a . The growth timescale for the embryos $\tau_{\text{c,acc}}$ also increases with a . On the gas depletion timescale τ_{dep} , the most massive embryos emerge near the ice line of a disk comparable to MMSN with a mass $M_c \sim M_{\text{iso}} < M_{\text{crit}}$ (Paper I). The magnitude of $M_{\text{iso}} \propto \Sigma_d^{3/2}$ and the embryos' characteristic growth time scale is $\tau_{\text{c,acc}} \propto \Sigma_d^{-1}$ (Kokubo & Ida 2002). In principle, M_{iso} can exceed M_{crit} in disks which are everywhere several times larger than the MMSN (Kokubo & Ida 2002; Thommes et al. 2007). But, the low efficiency of converting these building block material into embryos and few giant planets becomes a new issue. The retention of a large amount of heavy elements throughout the disk may also lead to noticeable metallicity dispersion among stars within any given stellar cluster, contrary to its observed upper limit (Wilden et al. 2002; Shen et al. 2005).

In order to resolve the issues of $M_p - a$ distribution and the adequacy of planet-building blocks, we consider an additional effect through which grains and planetary embryos may be trapped in some special location in the disk. This effect is associated with an intrinsic local pressure maximum in the disk which induces the gas to attain a super-Keplerian azimuthal speed. The hydrodynamic drag by the gas on the grains causes them to stall and become trapped near the ice line (Kretke & Lin 2007). In §2.1, we describe this grain trapping process and show how it may lead to the local (rather than global) enhancement of Σ_d near the ice line such that the formation of gas giants is possible in disks similar to the MMSN.

In Paper IV, we showed that the formation probability of gas giant planets and hence the predicted mass and semimajor axis distributions of extrasolar gas giants are sensitively determined by the strength of type I migration. Here we show that the structure of the disk near the ice line can also locally stall the type I migration of the embryos. In §2.2, we show that the modification of the azimuthal speed of the disk gas near the ice line provides another effective mechanism for the retention and rapid accumulation of embryos. In §3, we incorporate this effect into our numerical scheme and simulate the mass-semimajor axis

distribution of gas giant planets around solar-type stars. In §4, we summarize our results and discuss their implications.

2. Disk structure and heavy elemental retention

Gas giant planets form in protoplanetary disks prior to the gas depletion. The first step in this process is the condensation, growth, and retention of grains. In most regions of the disk, a negative pressure gradient in the radial direction reduces the azimuthal speed of the gas below the Keplerian value, so the grains undergo orbital decay (e.g., Adachi et al. 1976). At $a \sim 1$ AU in a MMSN, the meter-size particles migrate into the Sun within a few centuries. Particles can grow faster than their orbital decay provided the local Σ_d is larger than the surface density of gas Σ_g (Supulver & Lin 2001). Under these conditions and in the absence of turbulence in the disk, the grains may also settle into a thin layer and become gravitationally unstable (Safronov 1969; Goldreich & Ward 1973). However, Kelvin-Helmholtz instability caused by velocity difference between dust-rich and dust-poor layers (Weidenschilling & Cuzzi 1993; Sekiya 1998) and intrinsic turbulence such as Magneto-Rotational Instability (MRI) (Balbus & Hawley 1991) may prevent the concentration of dust grains. The main challenge in this scenario is how to enhance a local concentration of dust grains (Youdin & Shu 2002; Garaud & Lin 2004; Garaud 2007).

If the orbital decay of icy grains due to gas drag is terminated locally near the ice line, they would be concentrated near the ice line at orbital radius a_{ice} (eq. [9]). One possible mechanism to terminate their decay is through sublimation of icy dust grains and viscous diffusion of the water vapors across the ice line (Stevenson & Lunine 1988; Ciesla & Cuzzi 2006). Across a_{ice} , an equilibrium may be established in which the outward diffusion of water molecules and their recondensation into grains is balanced by the inward orbital decay of the solid particles. The exchange of latent heat associated with these phase transition significantly reduces the local temperature gradient (Kretke & Lin, in preparation). Here, we consider another possible mechanism to terminate the decay, positive radial gradient of disk gas due to change in activity of MRI across a_{ice} . This mechanism also halts type I migration of planetary embryos and enhances formation and retention rates of gas giants.

2.1. Layered-accretion and dust retention near the ice line

The magnitude of gas surface density Σ_g is determined by the efficiency of angular momentum transport in the disk. A leading mechanism for angular momentum transfer in

typical astrophysical disks is MRI. However, near the mid plane at a few AUs in protoplanetary disks, the gas may have a sufficiently low ionization fraction which quenches the MRI. This region is commonly referred to as the “dead zone” (Gammie 1996; Sano et al. 2000). Nevertheless, the surface layers of these disks are exposed to the ionizing photons from the central host stars and nearby massive stars (Glassgold et al. 1997) as well as cosmic rays. The ionization fraction χ in this layer is sufficient to provide an effective angular momentum transfer process which would allow an accretion flow with a flux $\dot{M} \sim 10^{-9} - 10^{-7} M_{\odot} \text{ yr}^{-1}$, which is inferred from observation of T Tauri stars (e.g., Hartmann et al. 1998). But, the magnitude of χ is determined by an ionization equilibrium which is determined by both the ionization and recombination rates. The main agents for removing electrons from the gas are grains (Sano et al. 2000; Turner et al. 2007). Interior to a_{ice} , the sublimation of ices greatly reduces the effective cross section of the grain population from that outside a_{ice} . Consequently, the active layer is much more extended interior to a_{ice} than exterior to a_{ice} .

The sublimation of ices at $r < a_{\text{ice}}$ implies that the angular momentum transfer efficiency in the surface layers undergo a transition across a_{ice} (Kretke & Lin 2007). In regions of disks well interior to the radius of maximum couple (Lynden-Bell & Pringle 1974), the disk flow (\dot{M}) rapidly adjusts to a state of quasi steady state in which \dot{M} is approximately independent of orbital radius r . In principle, the structure of a MRI-driven-turbulent disk requires multi-dimensional simulation, even in the limit of steady disk flow. Such simulations are time consuming and are yet to be fully resolved (Fromang & Papaloizou 2007; Fromang et al. 2007). In the present context, the dominant effects on the disk structure can be illustrated with the standard *ad hoc* α prescription to approximate the effective “turbulent viscosity” with $\nu = \alpha c_s h$, where c_s and h are sound velocity and scale height of the disk and α is an efficiency parameter (Shakura & Sunyaev 1973). In a steady accretion disk,

$$\dot{M} = 3\pi\nu\Sigma_g = 3\pi\alpha c_s h \Sigma_g. \quad (1)$$

In regions where the surface layer is sufficiently ionized to be affected by the MRI turbulence (Gammie 1996) but the interior is essentially shielded and remains inactive (or dead), we find it convenient to adopt a prescription by Kretke & Lin (2007) in which the effective magnitude of the α parameter,

$$\alpha = \frac{\Sigma_A \alpha_A + (\Sigma_g - \Sigma_A) \alpha_D}{\Sigma_g}, \quad (2)$$

where Σ_A is the gas surface density of the active layer and α_A and α_D are alpha parameters in MRI active and dead zones. Outside the ice line, the condensation of the grains significantly reduces the column density of the active layer. Since $\alpha_A/\alpha_D \gg 1$, the effective magnitude of α decreases as r across the ice line. In a quasi steady state where \dot{M} is nearly constant of r ,

$\Sigma_g \propto \alpha^{-1}$ so that Σ_g can be enhanced significantly across the ice line. This positive gradient of Σ_g can lead to a local pressure maximum.

When the exponent of disk midplane pressure P , defined by $s = d \log P / d \log r$, is positive, the grains experience a tail wind and the hydrodynamic drag leads to their outward orbital expansion (Nakagawa et al. 1986). For the equation of state of an ideal gas, $P \propto \rho_g T$, where ρ_g and T are mass density and temperature of the disk. Since $\rho_g \simeq \Sigma_g / 2h \simeq \Sigma_g \Omega_K / 2c_s$, where Ω_K is Keplerian frequency, positive s is realized when

$$p > -q/2 + 3/2, \quad (3)$$

where $p = d \log \Sigma_g / d \log r$ and $q = d \log T / d \log r$ ($d \log c_s / d \log r = q/2$). For $q = -1/2$, this condition is $p > 7/4$. A shallower surface density gradient is required if the release of the latent heat essentially suppresses the local temperature gradient.

Modification of the Σ_g profile is confined to the ice line region. Since the positive s is local, dust grains accumulate near the outer edge of the positive s region, which may lead to a large enhancement in Σ_d near the ice line region (Kretke & Lin 2007). Since the isolation core mass and the core's growth rate increases with Σ_d , it is possible to build up sufficiently massive cores to start the runaway gas accretion process while the residual gas is depleted to surface densities comparable to that of the MMSN.

2.2. Local pressure maximum and type I migration, planetesimal accumulation

Another important consequence for the modification of the rotation law is the suppression of type I migration efficiency (Masset et al. 2006). Even in the stage in which planet accretion from planetesimals proceeds, large amount of small dust grains may still float in the disk (Tanaka et al. 2005), so embryos undergoing type I migration can also be trapped near the ice line (Zhang et al. 2008).

For type I migration, since curvature of the system also affects the locations of Lindblad resonances, the condition for outward migration is slightly modulated from eq. (3). The migration rate of a planet with mass M_p is given by (Tanaka et al. 2002)

$$\frac{dr}{dt} \simeq 1.08(p + 0.80q - 2.52) \frac{M_p}{M_*} \frac{\Sigma_g r^2}{M_*} \left(\frac{r \Omega_K}{c_s} \right)^2 r \Omega_K. \quad (4)$$

This expression includes contributions from both Lindblad and corotation resonances. The dependence on q incorporates uncertainties associated with nonlinear effects. The condition

for outward migration is $p > -0.80q + 2.52$, which is similar to that for gas drag migration (eq. [3]). For $q = -1/2$, $dr/dt > 0$ for $p > 2.92$. As shown below, this condition can be satisfied near the ice line.

3. Simulations including the effect of ice line retention

3.1. Prescription in the numerical scheme

The dynamical evolution of the planetesimals is regulated by the surface density distribution of the gas in the disk. In principle, we should compute the evolution of the gas in terms of the standard diffusion equation which takes into account the gas infall, depletion, initial and boundary conditions. For computational convenience, we assume steady accretion flow and approximate

$$\dot{M} = 3 \times 10^{-9} f_{g,0} \exp(-t/\tau_{\text{dep}}) [M_{\odot}/\text{yr}], \quad (5)$$

and calculate evolution of Σ_g with eq. (1), by taking into account the effect of spatial non-uniformity of α . The value of $3 \times 10^{-9} M_{\odot}/\text{yr}$ is typical values of observed \dot{M} around stars with ages $\sim \text{Myr}$ (Hartmann et al. 1998). In this expression, we assume an exponential depletion of the disk gas on some characteristic depletion time scale (τ_{dep}). For the purpose of illustrating the gross effects of disk evolution on planets' migration, these approximations are adequate. However, we have not considered the aspect of non-steady nature of the flow which can lead to an outward type II migration at large distances from the host stars. Such an effect will be considered in the future.

Similarly, for computational convenience, we adopt a fiducial prescription for the initial surface density distribution of rocky and icy materials as in our previous papers such that

$$\Sigma_d = 10\eta_{\text{ice}} f_{d,0} (r/1\text{AU})^{-3/2} [\text{g}/\text{cm}^2], \quad (6)$$

where the enhancement factor (η_{ice}) is introduced to take into account the condensation of icy grains. In our previous papers, we simply set $\eta_{\text{ice}} = 1$ for $r < a_{\text{ice}}$ and $\eta_{\text{ice}} = 4.2$ for $r > a_{\text{ice}}$ according to Hayashi (1981). The phase transition between condensed and vaporized grains occurs over a small radial range, probably comparable to the vertical density scale height h . Here we smooth out the change in η_{ice} in terms of a tanh function with a width $\sim h$ (see Figs. 1). The enhancement factor may be slightly smaller (~ 3.0) (Pollack et al. 1994)]. We found that the retention efficiency of cores against type I migration is reduced only slightly and overall features of our results do not change, even if we use $\eta_{\text{ice}} = 3$ for $r > a_{\text{ice}}$ in our simulation, because a barrier for migration is a more important effect of the ice line than the enhancement of Σ_d .

In this paper, we consider the potential effect of Σ_g variation (due to changes in η_{ice}) across the ice line. In principle, we should take into account any possible accumulation of the trapped grains near the ice line prior to this seemingly arbitrary initial state. However, the local pressure maximum in the Σ_g distribution appears only after the gas accretion rate in the disk has declined below a critical value. Equation (6) corresponds to the surface density of the grains when this barrier at the ice line first appears. Thereafter, as grains congregate near the ice line, the ratio of Σ_d/Σ_g will increase. Eventually, the grains exert a significant torque on the gas to slow down its radial velocity (Nakagawa et al. 1986, Kretke et al. 2008). This process further modifies the Σ_g enhancement near the ice line.

In a turbulent disk, small (sub-mm) size grains are suspended in disks with scale height comparable to h . As Σ_d approaches to Σ_g , their collisional growth time scale reduces below their orbital evolution time scale (Supulver & Lin 2001). The vertical velocity shear in the disk is also reduced. Then modest ($>\text{mm}$) size grains can sediment from the turbulent surface layers to the more quiescent midplane regions of the disk and largest particles may settle to a sufficiently thin disk to eventually become gravitationally unstable, and form planetesimals (Youdin & Shu 2002), against the Kelvin-Helmholtz instability barrier (Weidenschilling & Cuzzi 1993). Possible molten surfaces of grains in this region may lead to sticky dust collisions, which also enhances dust sedimentation. The critical conditions for the onset of gravitational sedimentation and instability of the dust layer depend on the magnitude of Σ_d . In those models which we take into account the effect of accumulation of icy grains and water vapor near the ice line, we further increase η_{ice} in Σ_d (Fig. 1b) by a factor of

$$f_{\text{ice}} = [1 + 2 \exp(-(r - a_{\text{ice}})^2/h^2)]. \quad (7)$$

As shown later, the enhancement does not affect the results significantly, by the same reason of the case of $\eta_{\text{ice}} = 3$. We assume that dust grains have surface density that is comparable to that of planetesimals, in order to highlight the effect of the ice line.

Following the simple prescription of our previous papers, we adopt the equilibrium temperature in optically thin disk regions (Hayashi 1981),

$$T = 280 \left(\frac{r}{1\text{AU}} \right)^{-1/2} \left(\frac{L_*}{L_\odot} \right)^{1/4} \text{K}, \quad (8)$$

where L_* and L_\odot are the stellar and solar luminosity. The ice line is determined by this temperature distribution as

$$a_{\text{ice}} = 2.7 \left(\frac{L_*}{L_\odot} \right)^{1/2} \text{AU}. \quad (9)$$

Note that the magnitude of a_{ice} may be modified by the local viscous dissipation (Lecar et al. 2006) and stellar irradiation (Chiang & Goldreich 1997; Garaud & Lin 2007). The predicted

semimajor axis distribution of extrasolar planets reflects the magnitude of a_{ice} . Furthermore, a_{ice} changes with time due to disk evolution. The movement of the ice line may affect final mass and orbital configuration of planets (Kennedy et al. 2006; Kennedy & Kenyon 2008). Inclusion of this potentially important effect is left to a future paper. In the present paper, our purpose is to highlight the possibility of halting type I migration near the ice line and a great quantitative accuracy is not important.

3.2. Surface density distribution of the disk gas

From eqs. (2) and (5), Σ_g is given explicitly by

$$\Sigma_g = \frac{1}{\alpha_D} \left(\frac{\dot{M}}{10^{-8} M_\odot / \text{yr}} \right) \left(\frac{T_1}{300\text{K}} \right)^{-1} \left(\frac{r}{1\text{AU}} \right)^{-q-3/2} [\text{g}/\text{cm}^2] - \Sigma_A \left(\frac{\alpha_A - \alpha_D}{\alpha_D} \right), \quad (10)$$

where T_1 is disk midplane temperature T at 1AU. In Figures 1, the equilibrium Σ_g distributions are given as a function of \dot{M} . In this example, we adopt a set of assumed values $\alpha_A = 10^{-3}$, $\alpha_D = 10^{-4}$, and Σ_A where

$$\Sigma_A = \min \left(6\eta_{\text{ice}}^{-1} \left(\frac{r}{1\text{AU}} \right)^3 [\text{g}/\text{cm}^{-2}], \Sigma_g \right). \quad (11)$$

This prescription for Σ_A ($\Sigma_A < \Sigma_g$) is an order of magnitude higher than that adopted by (Kretke & Lin 2007). Although Kretke & Lin (2007) assumed μm -size grains, the ionization degree in the disk sensitively depends on grain sizes and the grain growth significantly enlarges the active layer (Sano et al. 2000; Turner et al. 2007). Dispersion in Σ_A due to the range of disk mass is generally smaller than variations in the dust growth properties. For the purpose of exploring and highlighting importance of the effect of the ice line, we use this high values of Σ_A .

Figures 1a and b show evolution of Σ_g without and with the enhancement of dust grains near the ice line. In the regions where $\Sigma_g \gg \Sigma_A$, the disk is mostly MRI dead and $\alpha \simeq \alpha_D$, while $\alpha \simeq \alpha_A$ in the $\Sigma_g \sim \Sigma_A$ regions. During early stages of disk evolution (epochs with high \dot{M}), the active surface layer occupies an insignificant fraction of the total disk, so the transition across a_{ice} does not modify the disk structure nor produce positive radial gradient. At advanced stages of disk evolution when Σ_g is very low ($\dot{M} < 10^{-9} M_\odot \text{ yr}^{-1}$), the active layer extends throughout the entire extent normal to the plane of the disk and the magnitude of Σ_g is also a monotonically decreasing function of r . However, for intermediate stages ($10^{-9} M_\odot \text{ yr}^{-1} \lesssim \dot{M} \lesssim 10^{-8} M_\odot \text{ yr}^{-1}$), the Σ_g distribution has a local maximum with positive gradient near the ice line. In the case with the Σ_d (f_{ice}) enhancement, the bump in

Σ_g is more pronounced. The power index for the Σ_g gradient is more than 2.9 near the ice line. Based on the consideration presented in §2.2, it is suggestive that type I migration of the planetesimals may be halted near there.

Note that the trapping efficiency of both grains and cores is determined only by the value of p and it does not depend on the amplitude of the surface density variation near the ice line. The most effective trapping location is interior to the ice line where the pressure gradient is most positive. The actual range of \dot{M} for effective ice-line barrier is a function of the poorly understood α_D . Furthermore, the size distributions of dust grains due to coagulation and fragmentation also regulate the magnitude of Σ_A and when the positive pressure gradient appears, but the evolution of the size distributions is also poorly understood. Nevertheless, the qualitative implication of this physical effect is unavoidable, the local pressure maximum near the ice line is essential for the retention of the planet-building blocks.

Figures 2 show the time evolution of planetesimals’ mass and semimajor axis for the model with $f_{g,0} = 3$ (without the Σ_d enhancement). For illustration purposes, the planetesimals’ initial semimajor axis distribution is chosen to be separated with equal logarithmic intervals. This figure shows that some cores are trapped near the ice line and grow there until they start to undergo efficient gas accretion.

3.3. Population synthesis

With these prescriptions, we carried out a series of Monte Carlo simulations to generate theoretical mass and semimajor axis distribution for extrasolar planets. Except for the disk gas surface density Σ_g and the q dependence of type I migration rate (see below), the formulae for growth and migration are identical to those in Paper IV.

We first generate a 1,000 set of disk models with various values of $f_{g,0}$ (the initial value of f_g) and τ_{dep} . In this paper, we focus on solar-type stars and consider a log uniform distribution for M_* in the range of 0.8–1.25 M_\odot . We assume $L_* = L_\odot (M_*/M_\odot)^4$ and $f_{g,0} \propto M_*^2$ (Paper III). These choices of M_* dependences do not significantly affect the results, because the range of M_* for these models is relatively narrow. The luminosity L_* also changes with time during pre-main sequence phase, in which planet formation proceeds. It affects the location of a_{ice} , but a_{ice} is affected more by disk structure, as mentioned in §3.1. So, we neglect evolution of L_* , for simplicity.

We also assume that τ_{dep} has a log uniform distribution in the range of 1-10 Myrs. This assumption is based on the observation that in young clusters within this age range, a fraction of coeval stars have signatures of disks and this fraction declines linearly with

the cluster age (Haisch et al. 2001). The modest dispersion in this fraction for clusters with similar ages is another indication that there is a considerable spread in the magnitude of τ_{dep} even in star forming regions with similar initial conditions.

We adopt the same prescriptions for the distributions of $f_{d,0}$ and $f_{g,0}$ as those in Papers II-IV. For the gaseous component, we assume $f_{g,0}$ has a log normal distribution which is centered on the value of $f_{g,0} = (M_*/M_\odot)^2$ with a dispersion of 1 ($\delta \log_{10} f_{g,0} = 1.0$) and upper cut-off at $f_{g,0} = 30$, independent of the stellar metallicity. For the heavy elements, we choose $f_{d,0} = 10^{[\text{Fe}/\text{H}]_d} f_{g,0}$, where $[\text{Fe}/\text{H}]_d$ is metallicity of the disk. We assume these disks have the same metallicity as their host stars. In this prescription, Σ_d throughout the entire disk varies with $[\text{Fe}/\text{H}]$ in contrast to the local enhancement near the ice line in some enriched models.

For each disk, 15 semimajor axes of the protoplanetary seeds are selected from a log uniform distribution in the ranges of 0.05–50AU. The averaged orbital separation between planets is 0.2 in log scale, or equivalently, the averaged ratio of semimajor axes of adjacent seed planets is $\simeq 1.6$.

For each set of $f_{g,0}$, $f_{d,0}$ and a values, we integrate the protoplanets' growth through planetesimal and gas accretions with semi-analytical prescriptions based on detailed numerical simulations. The initial mass is arbitrarily set to be a small value, $M_c = 10^{20}\text{g}$, albeit the orbital evolution of planets with such initial mass would not be affected by the effect of hydrodynamic drag. The choice of this initial mass does not affect the results because the accretion time scale for embryos with masses $> 10^{20}\text{g}$ increases with M_c , *i.e.*, they have entered the oligarchic growth phase.

In outer regions ($\gtrsim 10\text{AU}$), core growth is slow and scattering of planetesimals by the cores rather results in ejection from the systems, so *in situ* formation of giant planets is limited (Paper I). On the other hand, in inner regions, limited amount of planetesimals in feeding zones suppresses formation of giant planets (Paper I). Here, individual planets are integrated independently, neglecting dynamical interactions between them. Although the change in semimajor axis is not significant for inward scattering due to energy conservation, it can be very large for outward scattering. So, giant planets in outer regions would have been scattered from inner regions and they would have relatively large orbital eccentricities unless adequate damping has existed. Since the scattering process is not included in the current simulations, predicted distribution in outer regions would have uncertainty in outer regions. This should be cautioned when our current results are used for consideration of astrometric or direct imaging observations that are sensitive to planets in outer regions. The effect of the uncertainty is smaller for radial velocity observations that are sensitive to short-period planets, because these short-period planets would have undergone much

greater orbital migrations due to tidal interactions with disk gas (that are included in our simulations) than those due to the dynamical scattering. We will include the effects of dynamical interactions in a subsequent paper. This uncertainty does not affect the purpose of the present paper, highlighting the possibility of halting type I migration near the ice line.

We integrate the planets’ orbital evolution through type I and type II migrations in a disk with τ_{dep} around a star with M_* . The magnitude of f_d at a given location r continuously decreases with time from its initial value $f_{d,0}$ as planetesimals are accreted by embryos which in turn undergo orbital decay. Note that here the semimajor axis a is identified as orbital radius r , because we neglect evolution of orbital eccentricities. For the gas component, we adopt a prescription for an exponential decay with decay constant τ_{dep} as eq. (5).

While the type II migration speed is determined by an analytical formula with an empirical numerical factor (Paper IV), the type I migration speed is given with a scaling factor C_1 by

$$\dot{r} = C_1 \dot{r}_{\text{linear}}, \quad (12)$$

where \dot{r}_{linear} is given by eq. (4) with $q = -1/2$. The parameter p in the equation is calculated by Σ_g (eq. [10]) at each radius and each time. If the calculated p is larger than 2.92, the migration is outward. We regard C_1 as a parameter and do simulations for different values of C_1 . We artificially terminate type I and II migrations near disk inner edge where the orbital period of the planetesimals is 2 day ($\sim 0.03\text{AU}$ for $M_* = 1M_\odot$) in a similar manner as in Papers I-IV. (The fate of close-in planets will be examined in future investigations.)

In the present series of simulations, if a planet arrives at the inner edge, a next-generation planetary seed would be introduced. The evolution of this new planet would be integrated with the residual planetesimal surface density (see Paper IV). For many models, it is possible for several planets to reach the proximity of their host stars prior to the severe depletion of the disk gas. In all models, we record not only the individual close-in planets but also consider the limiting possibility that all the short-period planets around common host stars may undergo dynamical instability after the gas depletion, collide, and coagulate into a single entity (see §3.7).

3.4. Mass and semimajor axis distributions

In equation (12), C_1 represents a reduction factor. For exploration purpose, we consider models with C_1 in the range of 0-1. The predicted $M_p - a$ distributions of extrasolar planets is shown in Figures 3 for $C_1 = 0.03, 0.1, 0.3$, and 1. Figures 3a are the results of models in which we have neglected the ice-line barrier. In the absence of a Σ_g bump near the ice line,

we assume $\Sigma_g = 750 f_{g,0} \exp(-t/\tau_{\text{dep}})(r/1\text{AU})^{-1} [\text{g/cm}^2]$ and $\alpha = 10^{-3}$ throughout the disk.

In contrast, the simulated results for models that explicitly include the ice line barrier are shown in Fig. 3b (without the Σ_d enhancement) and c (with the Σ_d enhancement by a factor of f_{ice} as eq. [7]). We adopt $[\text{Fe}/\text{H}] = 0.1$ for all these models because the on-going radial velocity surveys have been focusing on relatively metal-rich stars. ($[\text{Fe}/\text{H}]$ -dependence is shown in §3.6.) To compare with the theoretical prediction and the data of radial velocity observations, we also plot the data of all planets (discovered by radial velocity surveys), around stars with $M_* = 0.8\text{--}1.25 M_\odot$. In order to correct for the projection effect, we adopted $4/\pi$ ($\simeq 1.27$) for the $1/\sin i$ factor.

First, we discuss the simulated results in which the ice line barrier has been neglected (Fig. 3a). These results are essentially the same as those in Paper IV, except that in our previous simulations, we adopted $M_* = 1 M_\odot$ without any dispersion. In the absence of any ice line barrier, only for $C_1 \lesssim 0.03$ (*i.e.* in the inefficient type I migration limit), the predicted population of gas giants matches well with the observed data (see below). In models with higher values of $C_1 (> 0.3)$, only the low-mass ($M_p < 10 M_\oplus$) cores can survive the type I migration. These low-mass cores cannot evolve into gas giants because their envelope contraction time scales are generally much longer than the gas depletion time scales (Paper IV).

We now consider the influence of the ice-line barrier. In a series of models with a Σ_g bump (Figs. 3b and c), much larger populations of gas giants are generated than the barrier-free models with corresponding values of C_1 (Fig. 3a). Furthermore, in these models, the semimajor axis distribution of gas giants shows a ramp up in the planetary population with $a \sim 1\text{--}3\text{AU}$ (Figs. 3b and c). Although in the limit of small C_1 , gas giants can also form without the ice line barrier, their a distribution is essentially logarithmic (Figs. 3a, also see Paper I).

This dichotomy can be attributed to the role of the ice-line barrier which is to preserve cores until they become sufficiently massive (with $M_c \sim 10 M_\oplus$) to efficiently accrete gas. Planetesimals formed at large distances from their host stars migrate inward and become trapped near the ice line. They accumulate and coagulate into embryos at this barrier until either the disk gas is depleted or they attain a critical mass to initiate efficient gas accretion. However, planetesimals formed interior to the ice line cannot halt their inward type I migration until they have reached the proximity of their host stars. If these close-in planets are embedded in residual gas, their eccentricities would be effectively damped and their further growth would be inhibited by dynamical isolation. After the severe depletion of the disk gas, dynamical instability can lead to orbit crossing, cohesive collisions, and emergence of relatively massive short-period planets. Although some of these cores may have

$M_c > 10M_\oplus$, the depletion of gas would prevent the build up of their envelopes. Around solar type stars, it is difficult for gas giants to form in close-in orbits.

After they have acquired planet masses comparable to those of Jupiter and Saturn, gas giants formed near the ice line barrier open gaps and undergo type II migration (Figures 2). However, since the ice line barrier is only effective for a range of modest $\dot{M} \sim 10^{-9} - 10^{-8} M_\odot \text{ yr}^{-1}$, most gas giants emerge in relatively passive disks and the extent of their migration is somewhat limited. Consequently, the fraction of stars with short-period gas giants (η_{sJ}) is much reduced in the models with the ice-line barrier than the low- C_1 models in which the ice-line barrier effect is neglected (see further discussions in §3.7). Since the magnitude of η_{sJ} predicted with these new models is comparable to its observed value ($\sim 1\%$), we no longer need to invoke extensive disruption mechanisms for the excess predicted short-period gas giants. The reduction in the gas giants’ type II migration, due to their late emergence, also helps to preserve the upturn in their a (or P) distribution which is a signature of their formative environment rather than some evolutionary outcomes. Overall, these simulated results are in a better agreement with the observed data.

There are also many cores trapped near the ice-line barrier which do not have sufficient mass to accrete gas prior to its severe depletion. When \dot{M} reduces below $\sim 10^{-9} M_\odot \text{ yr}^{-1}$, these cores resume their type I migration due to the removal of the ice line barrier. However, the magnitude of Σ_g of the residual gas is generally too low for the initially trapped cores with $M_c \sim$ a few M_\oplus to undergo extensive migration. This modest population of rocky planets reside close to the habitable zone (hereafter HZ) slightly interior (at 1-3 AU) to the ice line barrier region (see further discussions in §3.7). Since these cores form in nearly isothermal regions where gas-phase-vapors and solid-phase-ice coexist, they may contain a substantial amount of life-supporting water. The orbits of a fraction of these rocky planets may be destabilized by coexisting gas giants in the same systems. But around host stars without any gas giants, their orbital eccentricity may be damped by their interaction with the residual planetesimals.

Despite the production of occasional intermediate-mass ($M_c \sim$ a few M_\oplus) planets at \lesssim a few AU, a characteristic “planet desert” (see Paper I) is still prominent in Figures 3b and c. The boundaries of the desert domain are modified by the efficiency of the barrier. Since the ice-line barrier cannot act to preserve them, low-mass ($M_c < M_\oplus$) planetesimals and embryos formed interior to it migrate to the proximity of their host stars in the presence of relatively small amount of residual disk gas.

We now consider the influence of initial Σ_d enhancement near the ice-line barrier. As we stated in the introduction, $M_{\text{iso}} \propto \Sigma_d^{3/2}$ and $\tau_{\text{c,acc}} \propto \Sigma_d^{-1}$. In principle, the enhancement of Σ_d by a factor of f_{ice} near the ice line leads to rapid growth of embryos with relatively

large isolation masses. In the comparisons between these two series of models, we find that the distributions of gas giants are similar, albeit a f_{ice} enhancement leads to the emergence of marginally more detectable planets, especially in the limit of modest values of $C_1 (\gtrsim 0.3)$. The weak dependence is also partially caused by the ice-line barrier being effective only after $\dot{M} < 10^{-8} M_{\odot} \text{ yr}^{-1}$ so that relatively massive embryos which emerged during earlier epochs of active disk evolution would not be preserved. This self-regulated retention condition reduces the advantage of the initially more massive disks. The principle factor for the formation probability of gas giants is the existence of the ice line barrier rather than any localized initial concentration of Σ_d .

3.5. Enhancement of formation probability of gas giants and domain of planetary desert

In order to quantitatively compare with observations, we determine the fraction (η_J) of stars which harbor planets within the present radial-velocity detectability limit. Following Fischer & Valenti (2005), we take a conservative estimate on the magnitude of radial velocity ($v_r > 10 \text{ m/s}$) and orbital periods ($T_K < 4$ years) for the detectable conditions. Because we artificially terminate type I and II migrations near disk inner edge and we have not specified a survival criterion for the close-in planets, we exclude close-in planets with $a < 0.05 \text{ AU}$ in the evaluation of η_J . (see further discussions on the short-period planets in §3.7).

The values of η_J are plotted as a function of C_1 in Figure 4a. The dependence of η_J on C_1 is much weaker among models which take into account the ice line effect than those without it. Even for $C_1 = 0.3\text{--}1$, the predicted η_J can be comparable to the observed data (Fischer & Valenti 2005). Migrating cores are trapped near the ice line, almost independent of the strength of type I migration, and they accrete planetesimals until either 1) they can start runaway gas accretion or 2) Σ_g near the ice line is reduced below Σ_A and they resume their type I migration. The coupling effect of MRI activity and the ice line barrier can enhance formation and retention rates of gas giants without significant reduction of the strength of type I migration.

A close inspection of Figures 2 shows that although the paucity of intermediate-mass intermediate-period planets is maintained, the evacuation of this planetary desert is less severe in the series of models with the ice-line barrier than those which neglected this effect. The upper M_p boundary of the desert shifts downward with increasing C_1 and $f_{d,0}$ where a large a limit extends to the HZ. A few planets emerge in this sparsely populated region and some of them have masses and orbits similar to those of the Earth. In order to extrapolate the probability of finding habitable planets from the known extrasolar planets, we adopt the

Terrestrial Planet Finder’s convention for the domains of habitable planets (Des Marais et al. 2002). We plot in Figure 4b the fraction of stars with habitable planets (η_{\oplus}) which is defined as planets with $M_p \simeq 0.3 - 10M_{\oplus}$ and $a \simeq 0.75 - 1.8$ AU around G dwarfs.

These planets are formed in the ice line barrier region of those disks which contain a marginal amount of heavy elements. Their progenitors’ growth toward super-earth-mass cores is slow. When they finally acquired sufficient masses to efficiently accrete gas, the magnitude of Σ_g near their orbits also decreases below Σ_A such that the residual disk does not have adequate mass to promote these protoplanets to attain their full growth potential prior to the severe gas depletion. However, a relatively small Σ_g is needed to induce the super-earth-mass cores to undergo fractional orbital decay. The late “leakage” of a few cores into the planetary desert does not significantly alter the landscape of the planetary desert, albeit the presence of a few intermediate-mass intermediate-period planets is no longer forbidden (also see previous subsection).

3.6. Metallicity dependence

Based on the assumption that protostellar disks attain the same fraction of heavy elements as that contained in their host stars, we showed, in Paper II, that gas giant planet formation is more prolific around metal-rich than metal-poor stars. In addition to the availability of planet building blocks, disks with enhanced metallicities also contain a greater population of grains which can modify the ionization fraction, the depth of the active layer, and potentially the retention efficiency of the ice-line barrier. But the range of \dot{M} over which the ice line barrier is effective does not depend explicitly on the magnitude of the metallicity.

Figure 5 shows the values of η_J which are plotted as a function of $[\text{Fe}/\text{H}]$. Open circles with error bars are observational data compiled by Fischer & Valenti (2005). Triangles with dotted line shows the results without type I migration, which are based on similar results to those shown by Paper IV. The correlation reflects the fact that higher $[\text{Fe}/\text{H}]$ enhances formation of cores large enough for runaway gas accretion through higher $\Sigma_{d,0}$. In Paper IV, we suggested that the effect of type I migration enhances the η_J – $[\text{Fe}/\text{H}]$ correlation, because type I migration is more efficient in metal-poor disks. Squares with dashed line represent the results from models in which type I migration with $C_1 = 0.03$ is included and the ice line barrier is neglected. A modest η_J amplitude and its steep $[\text{Fe}/\text{H}]$ dependence are in a better agreement with the observed data (Fischer & Valenti 2005) than the models in which the effects of type I migration has been altogether neglected (represented by triangles and dotted lines).

We now consider models in which the ice-line barrier is taken into account. The filled pentagons and circles with solid lines respectively represent models without and with the $\Sigma_{d,0}$ enhancement at the ice line. Despite an order of magnitude increase in the value of $C_1 (= 0.3)$, the magnitude of η_J for the ice-line barrier models is comparable to or larger than those in which the ice line barrier effect is neglected.

We note from the comparison of the pentagon and filled-circle data points that the magnitude of η_J increases $\Sigma_{d,0}$ by a similar factor for all metallicity. This trend is another indication that the ice-line barrier essentially suppresses the depletion by type I migration effect once the gas surface density decreases below Σ_A . The greater availability of planet-building blocks enhances the probability of gas giant formation in these models.

3.7. Short-period planets

In paper IV, we carried out a survey of short-period planets which can migrate to within 0.03 AU from their host stars. In Figures 6, we plot mass functions of short-period planets in the cases (a) without the ice-line barrier, (b) with the ice-line barrier and no Σ_d enhancement, and (c) with the ice-line barrier and the Σ_d enhancement. In the upper panels, we assume that all the short-period planets survive without any further coagulation near their host stars. After the severe depletion of the disk gas, however, dynamical instability may develop and induce the coagulation of planets. In the lower panels, we consider the limiting case that around individual host stars, all planetesimals migrate to their proximity would merge into one short-period planet.

If we neglect the ice-barrier (the upper panel in Figure 6a), the mass distribution of these short-period planets would be biased toward Jupiter mass for $C_1 \lesssim 0.001$ (filled circles). However, even with a relatively small but finite value of $C_1 (\gtrsim 0.01)$, there would be a population of Earth-mass planets. For $C_1 \sim 0.01$, the resultant mass function of the short-period planets would be bimodal. For $C_1 > 0.1$, formation of gas giants is inhibited so that the mass function is highly peaked at a few M_\oplus 's.

This dichotomy is clearly demonstrated in the upper panel in Figure 7a where the short-period planets are classified into three populations. The filled circles, squares, and triangles represent the fraction of stars (η_s) which bear short-period planets with M_p in the range of $> 100M_\oplus$, $20 - 100M_\oplus$, and $1 - 20M_\oplus$, respectively. The population of planets with $M_p > 100M_\oplus$ rapidly decreases with C_1 , while that of smaller planets decreases more slowly. The observed value of $\eta_{s,J} \equiv \eta_s(M_p > 100M_\oplus) \sim 1\%$ can be matched with $C_1 \sim 0.1-0.3$, provided most short-period planets are retained.

In these models, $C_1 \lesssim 0.03$ is needed to match η_J of all the gas giant planets and the over-prediction of η_s can still match its observed value under the assumption that more than 95% of the short-period gas giants have perished. There are also a similar population of intermediate mass ($10 - 100M_\oplus$) and a much larger population of earth-mass short-period planets. If all the planets which migrated to the proximity of their individual host stars can subsequently collide and merge, the intermediate and low mass planets would become the building blocks of the massive short-period planets (see the lower panels in Figures 6a and 7a). But such planets are mostly composed of rocky cores rather than an extended envelope and HD 149026b (Sato et al. 2005) is a good candidate for such massive mostly rocky short-period planets. In order to match the observed value of η_{sJ} , most of these planets must be lost to their host stars.

We now consider the statistical outcome of short-period planet formation in the limit that type I migration is suppressed by the ice-line barrier. This process not only promotes the emergence of Jupiter-like gas giants but also introduces a strong modification in the mass function of the short-period planets (see Figs. 6b and c). The effect of the Σ_d enhancement is small in the function. Compared with Fig. 6a, the dependence on C_1 is very weak with the ice-line barrier. The magnitude of the observed value of η_J can be matched with $C_1 \sim 0.1 - 1$ (see Fig. 4a and the middle panels of Figs. 3b and c). With this range of parameter, the model values of η_s for gas giants (circles) are also comparable to that observed, provided some of them have coagulated and most of them have been retained in the proximity of their host stars. The magnitude of $\eta_s(M_p)$ (Figs. 7b and c) and the mass distribution of the short-period planets (Figs. 6b and c) indicate that there is a comparable or larger population of short-period intermediate-mass ($20 - 100M_\oplus$) planets as that of short-period gas giants. Since the value of M_p for the peak of the mass distribution is a function of C_1 , its determination can provide valuable calibration for the theoretical models.

The retention efficiency of the short-period planets remains uncertain. Several halting mechanisms have been proposed for the short-period planets. They include planet-star tidal interaction, magnetospheric cavity, Roche-lobe overflow, and trapping at surface density transition zones (Lin et al. 1996; Trilling et al. 1998; Gu et al. 2003; Masset et al. 2006; Laine & Lin 2008). Although the efficiency of these processes is to be determined in the future, the lower mass rocky planets are more likely to survive than the gas giants in most of these scenarios. Thus, we anticipate the prolific discovery of intermediate to low mass close-in planets in the near future searches. We predict the fraction of stars which bear short-period earth-mass ($\eta_{sE} \equiv \eta_s(M_p = 1 - 20M_\oplus)$) is comparable to that of all gas giants (η_J). This result is insensitive to the initial surface density distribution of the heavy elements ($f_{d,0}$).

Based on these results and the calibration of η_J for all known planets, we extrapolate $\eta_{\oplus} \sim 5\text{--}20\%$ depending on the magnitude of C_1 . The magnitude of η_{\oplus} can be reduced by perturbations from gas giants that we have not taken into account in our analysis. However, as stated before, for relatively large C_1 , the reduction would be small.

4. Summary and Discussions

In this paper, we confronted two main outstanding challenges to the core accretion scenario: 1) the efficient utilization of planets' building block material and 2) the retention of cores to form gas giant planets despite the hydrodynamic drag by the disk gas on grains and the orbital decay of the protoplanetary cores due to their tidal interaction with the disk gas (type I migration). We propose that the resolution of these conundrums lies in the existence of an ice line barrier.

In our scenario, we identify the ice line as a transition zone for the efficiency of angular momentum transfer in the gas disk. The presence of additional grains outside the ice line reduces the thickness of the active layer and the efficiency of angular momentum transfer. Within a range of the disk mass accretion rate (\dot{M} comparable to that observed for the classical T Tauri stars), these effects lead to local maxima in the pressure and surface density distribution in the disk. In the region slightly interior to ice line (closer to the star), a super-Keplerian gas flow provides a barrier to retain the heavy elements. Consequently, protoplanetary embryos coagulate and grow in mass at this location. Up on acquiring several M_{\oplus} , these cores initiate efficient gas accretion and evolve into gas giants. Since this ice line barrier is effective over a range of modest mass transfer rate ($10^{-9} - 10^{-8} M_{\odot} \text{ yr}^{-1}$), it regulates the formation of the first-generation gas giants during a preferred epoch at a preferred location around their host stars.

In relatively massive disks, the emergence of the first-generation planet leads to gap formation. Just beyond the outer edge of gap, another pressure maximum is induced. Similar to the ice line, this local pressure maximum promotes the congregation, coagulation, and rapid growth of later generations of gas giants. However, the physical extent of the planetary system is limited to the region where the local Keplerian speed is comparable to the surface escape speed of the critical mass (a few M_{\oplus}) cores. Outside this location, close (non collisional) encounters by these cores lead to ejection of their neighboring planetesimals from the system so that the depletion of the building block material is faster than the cores' growth.

Although gas giant formation is inhibited in relatively low-mass disks, they may nonethe-

less be the birth places of Earth-mass rocky planets in habitable zones as well as in the proximity of their host stars. The final assemble of these planets may proceed throughout the age of their host stars. While, in the post T Tauri phase, there is still small amount of residual gas in the disk, many of these entities may undergo type I migration over limited radial range towards their host stars. After the disk gas is severely depleted, these planets destabilize each other's orbits, albeit the eccentricities of the most massive planets may be suppressed by their gravitational interaction with the less massive residual planetesimals.

Through physical collisions, a population of a few- M_{\oplus} planets is expected to emerge in the habitable zone around 5-20 % of solar type stars. Some close encounters can also lead to limited migration. Nevertheless, a desert in the $M_p - a$ distribution is likely to be preserved. The paucity of planets with intermediate mass and semi major axis can be established with various observational surveys in the next few years. The boundaries of this domain contain valuable information on the efficiency of various process and valuable calibrations for the theoretical models.

Many planetesimals and embryos migrate to the proximity of their host stars, especially in the limit of relatively efficient type I migration. Many cohesive collisions may also occur among these planetesimals and embryos in the proximity of their host stars. Provided most of these planets are retained (despite the effect of their interaction with the magnetosphere and tide of their host stars), we anticipate the fraction of solar type stars with short-period earth-mass objects to be several times that of short-period gas giants. The physical composition of these close-in planets is most likely to be rocky to icy. Their observed mass distribution will enable us to calibrate the magnitude of the type I migration (the magnitude of C_1). The next step is to extrapolate and to calibrate the fraction of low-mass M-dwarfs and high-mass G sub-giant stars which may bear potentially habitable planets.

ACKNOWLEDGMENTS. We thank Katherine Kretke for providing the critical prescription of the disk structure model. We also thank A. Cumming, G. Laughlin, G. Marcy, N. Turner, and X.J. Zhang for useful conversation and a referee for helpful comments. This work is supported by NASA (NAGS5-11779, NNG06-GF45G, NNX07A-L13G, NNX07AI88G), JPL (1270927), NSF(AST-0507424), and JSPS.

CORRESPONDENCE should be addressed to S. I. (ida@geo.titech.ac.jp).

REFERENCES

- Adachi, I., Nakazawa, K., & Hayashi, C. 1976, PASJ, 29, 163
- Balbus, S. A., & Hawley, J. F. 1991, ApJ, 376, 214
- Chiang, E. I. & Goldreich, P. 1997, ApJ, 490, 368
- Ciesla, F. J. & Cuzzi, J. N. 2006, Icarus, 181, 178
- Cumming, A. Marcy, G.W. Butler, R.P. Fischer, D.A. Vogt, S.S. & Wright, J.T. 2008, in preparation.
- Des Marais, D. J. Harwit, M. O. Jucks, K. W. Kasting, J. F. Lin, D. N. C. Lunine, J. I. Schneider, J. Seager, S. Traub, W. A.; Woolf, N. J. 2002, AstroBio, 2, 153
- Fischer, D. A. & Valenti, J. A. 2005. ApJ, 622, 1102
- Fromang, S. & Papaloizou J. 2007, A&A, 476, 1113
- Fromang, S. Papaloizou J. Lesur, G. & Heinemann, T. 2007, A&A, 476, 1123
- Gammie, C. F. 1996, ApJ, 457, 355
- Garaud, P. 2007, ApJ, 671, 209
- Garaud, P. & Lin, D. N. C. 2004, ApJ, 608, 1050
- Garaud, P. & Lin, D. N. C. 2007, ApJ, 654, 606
- Goldreich, P., & Tremaine, S. 1980, ApJ, 241, 425
- Goldreich, P., & Ward, W. R. 1973, ApJ, 183, 1051
- Glassgold, A. E., Najita, J. & Igea, J. 1997, ApJ, 480, 344
- Gu, P., Lin, D. N. C., & Bodenheimer, P. H. 2003, ApJ, 588, 509
- Haisch, K. E., Lada, E. A. & Lada, C. J. 2001, ApJ, 553, L153
- Hartmann, L., Calvet, N., Gullbring, E., & D'Alessio, P. 1998, ApJ, 495, 385
- Hayashi, C. 1981, Prog. Theor. Phys. Suppl., 70, 35
- Ida, S. & Lin, D. N. C. 2004, ApJ, 604, 388 (Paper I)
- . 2004, ApJ, 616, 567 (Paper II)

- . 2005, *ApJ*, 626, 1045 (Paper III)
- . 2008, *ApJ*, 673, 487 (Paper IV)
- Kokubo, E. & Ida, S. 2002, *ApJ*, 581, 666
- Kennedy, G. M., Kenyon, S. J. & Bromley, B. C. 2006, *ApJ*, 650, L139
- Kennedy, G. M. & Kenyon, S. J. 2008, *ApJ*, 673, 502
- Kretke, K. A. & Lin, D. N. C. 2007, *ApJ*, 664, L55
- Kretke, K. A. Lin, D. N. C. Turner, N. & Garaud, P. 2008, *ApJ*, submitted
- Laine, R. & Lin, D. 2008, *ApJ*, submitted.
- Lecar, M., Podolak, M., Sasselov, D. & Chiang, E. 2006, *ApJ*, 640, 1115
- Lin, D. N. C., Bodenheimer, P. & Richardson, D. 1996, *Nature*, 380, 606
- Lynden-Bell, D. & Pringle, J. E. 1974, *MNRAS*, 168, 603
- Masset, F. S., D’Angelo, G., Kley, W., 2006, *ApJ*, 652, 730
- Nakagawa, Y., Sekiya, M. & Hayashi, C. 1986, *Icarus*, 67, 375
- Pollack, J. B., Hollenbach, D., Beckwith, S., Simonelli, D. P., Roush, T., & Fong, W. 1994, *ApJ*, 421, 615
- Quillen, A. C. 2002. *AJ*, 124, 400
- Safronov, V. 1969, *Evolution of the Protoplanetary Cloud and Formation of the Earth and Planets* (Moscow: Nauka Press)
- Sano, T., Miyama, S. M., Umebayashi, T., & Nakano, T., 2000, *ApJ*, 543, 486
- Sato, B., et al., 2005 *ApJ*, 633, 465
- Sekiya, M. 1998, *Icarus*, 133, 298
- Shakura, N. I. & Sunyaev, R. A. 1973, *A&A*, 24, 337
- Shen, Z.-X., Jones, B., Lin, D. N. C., Liu, X.-W., Li, S.-L. 2005, *ApJ*, 635, 608
- Stevenson, D. J. & Lunine, J. I. 1988, *Icarus*, 75, 146
- Supulver, K. D. & Lin, D. N. C. 2001, *Icarus*, 146, 525

- Tanaka, H., Takeuchi, T. & Ward, W. 2002, ApJ, 565, 1257
- Tanaka, H., Himeno, Y. & Ida, S. 2005, ApJ, 625, 414
- Thommes, E.W. Nilsson, L. & Murray, N. 2007, ApJ, 656, L25
- Trilling, D. E., Benz, W., Guillot, T., Lunine, J. I., Hubbard, W. B. & Burrows, A. 1998, ApJ, 500, 428
- Turner, N. J., Sano, T., Dziourkevitch, N. 2007, ApJ, 659, 729
- Ward, W. 1986, Icarus, 67, 164
- . 1993, Icarus, 106, 274
- Weidenschilling, S. J. & Cuzzi, J. N. 1993 Protostars and Planets II, ed. V. Mannings, A. P. Boss & S. S. Russell (Tuscon: Univ. of Arizona Press), 1031
- Wilden, B. S., Jones, B. F., Lin, D. N. C., Soderblom, D. R. 2002, AJ, 124, 2799
- Youdin, A. N. & Shu, F. H. 2002, ApJ, 580, 494
- Zhang, X.J. Kretke, K. & Lin, D.N.C. 2008, in *Proceedings of IAU Symposium 249: Exoplanet: Detection, Formation and Dynamics.*, eds Y.S.Sun, S.Ferraz-Mello, J.L.Zhou, Cambridge University Press: Cambridge
- Zhou, J.-L., Aarseth, S. J., Lin, D. N. C. & Nagasawa, M. 2005, ApJL, 631, L85

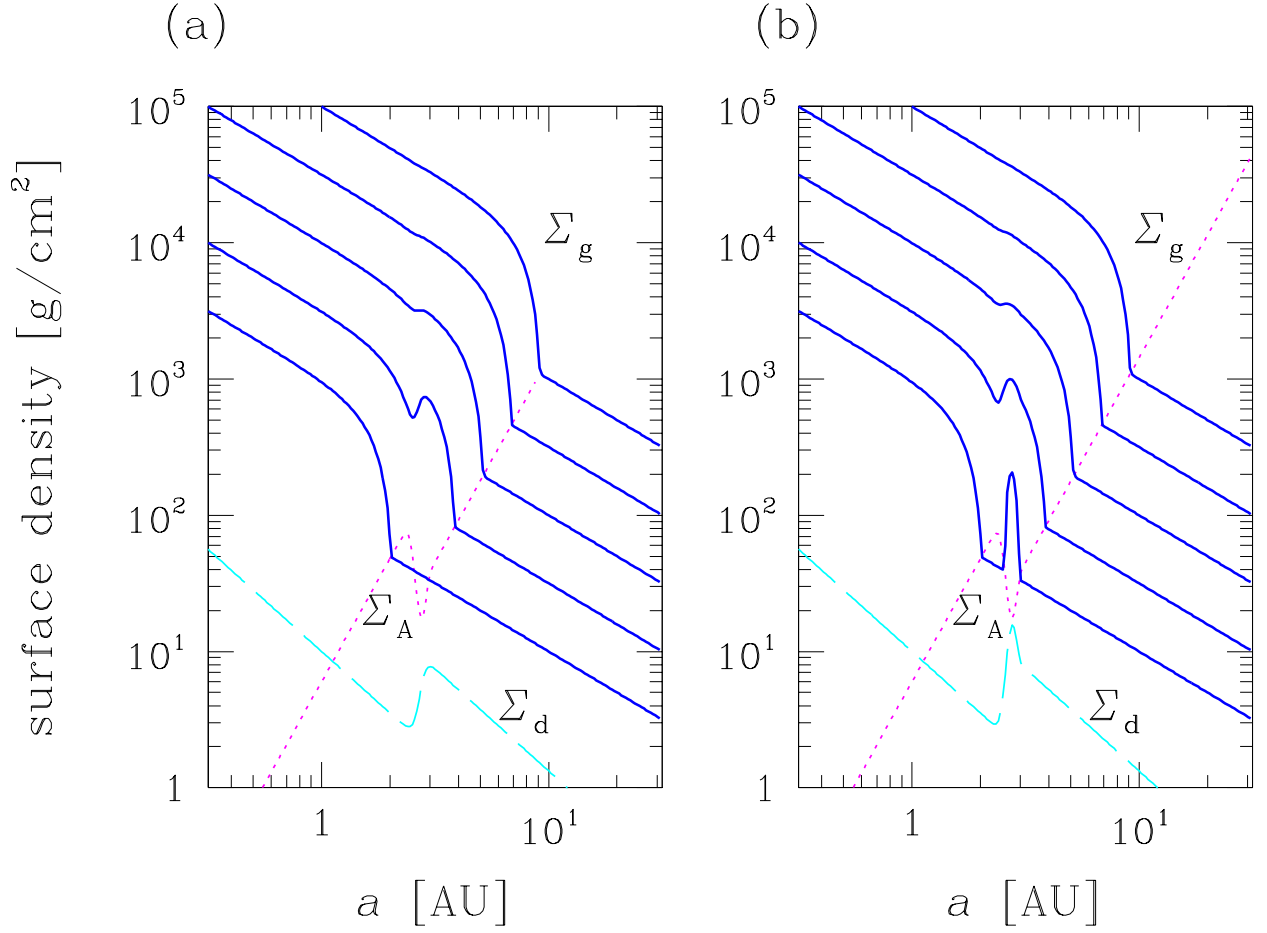


Fig. 1.— The evolution of equilibrium Σ_g distributions with the coupling effect of MRI and the ice line. The distributions (a) without the effect of enhancement in Σ_d due to the grain trapping and (b) with the effect. The solid lines express the Σ_g distributions for $\dot{M} = 10^{-7}, 3 \times 10^{-8}, 10^{-8}, 3 \times 10^{-9}, 10^{-9} M_\odot/\text{yr}$ from top to bottom. The dotted and dashed lines are Σ_A and Σ_d with $f_d = 1$.

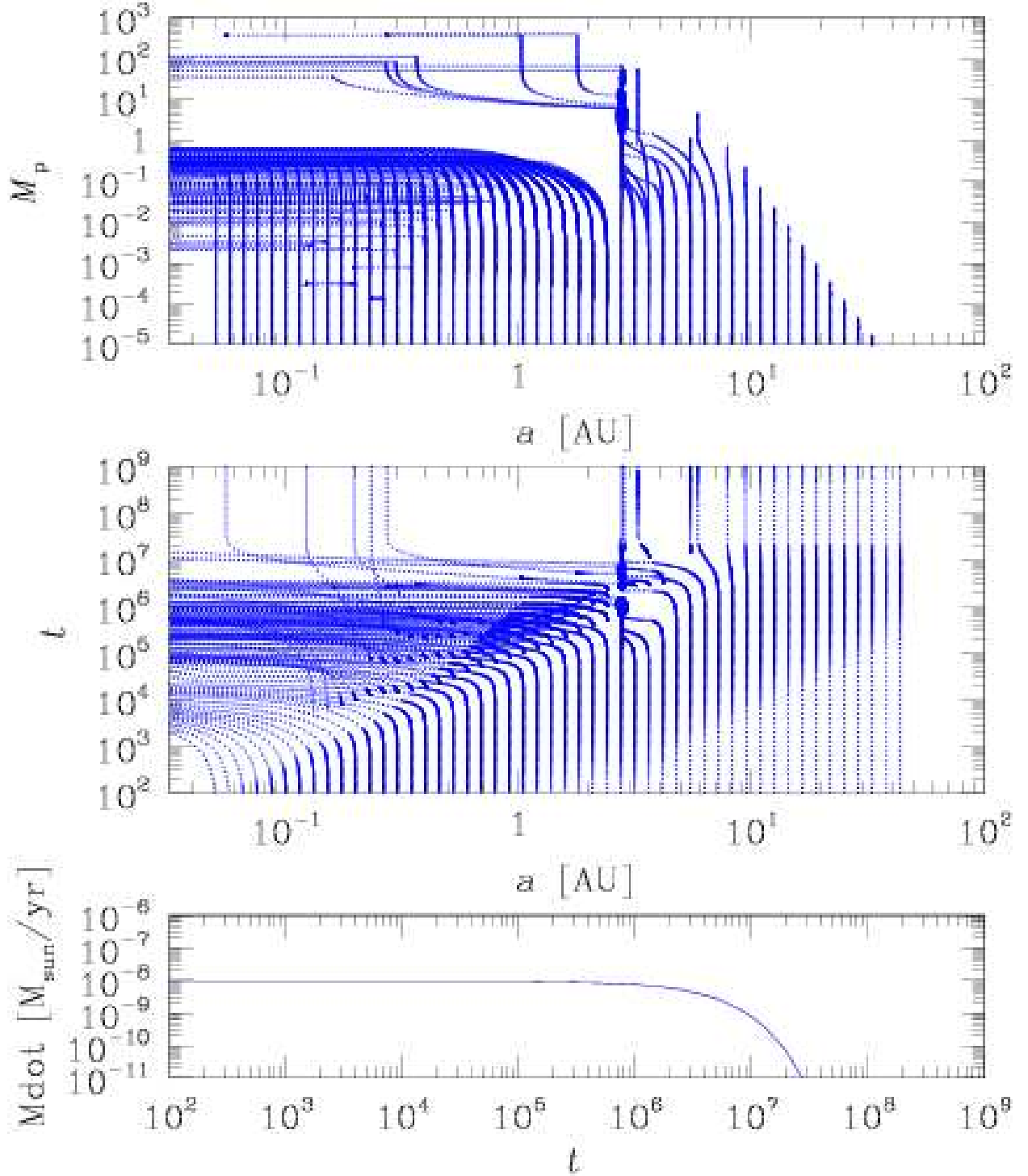


Fig. 2.— The time evolution of planetesimals’ mass (M_p) and semimajor axis (a) for the case of Fig. 1. Here, $f_{g,0} = 3$ and $\tau_{\text{dep}} = 3 \times 10^6$ years. The bottom panel shows time evolution of \dot{M} .

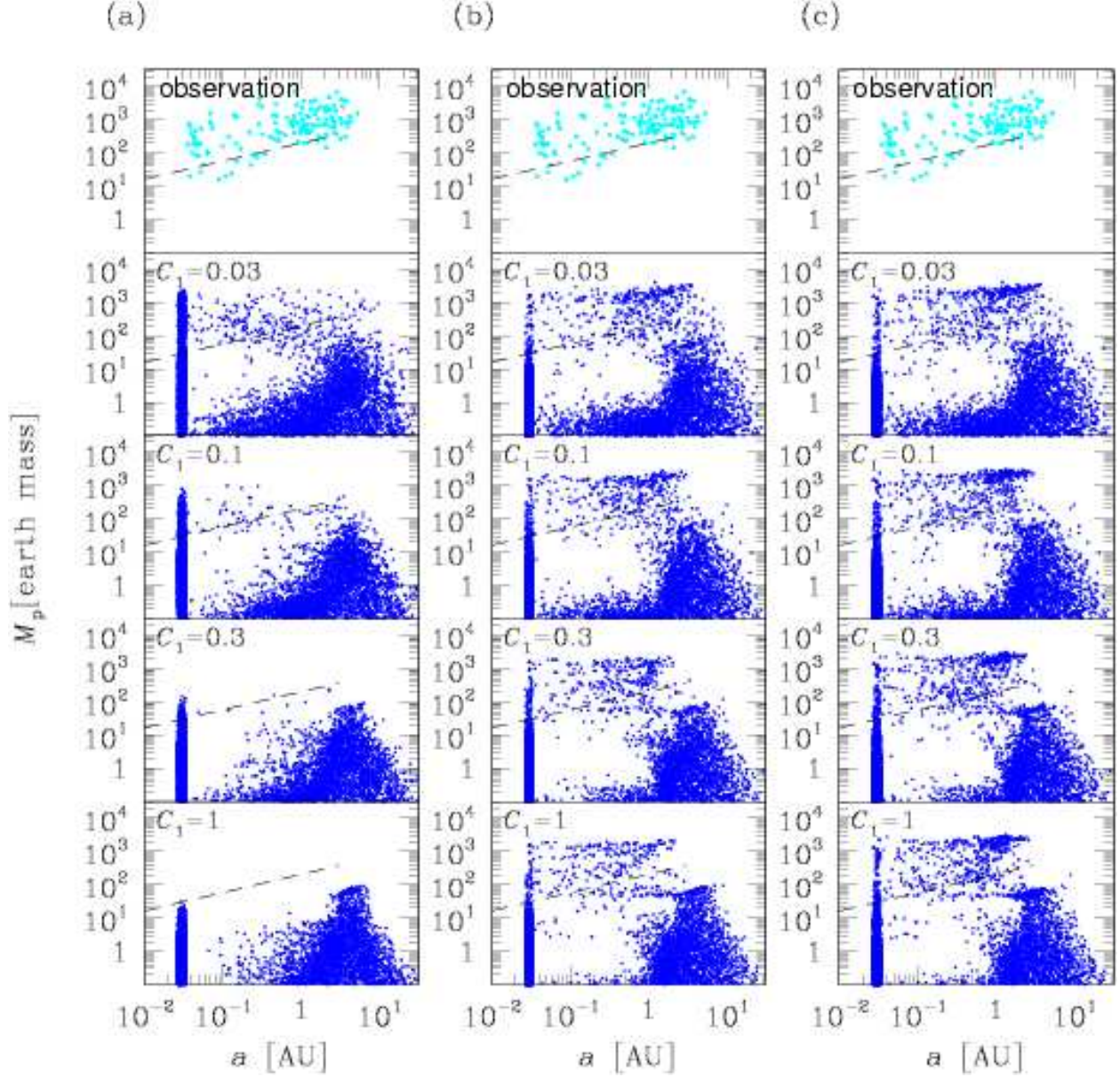


Fig. 3.— The mass and semimajor axis distribution of extrasolar planets. Units of the mass (M_p) and semimajor axis (a) are earth mass (M_\oplus) and AU. (a) The results in disks without the Σ_g bump due to the coupling effect of MRI activity and the ice line, (b) those with the bump in Σ_g but without the Σ_d enhancement, and (c) those with both the effects. The top panels are observational data of extrasolar planets (based on data in <http://exoplanet.eu/>) around stars with $M_* = 0.8\text{--}1.25M_\odot$ that were detected by the radial velocity surveys. The determined $M_p \sin i$ is multiplied by $1/\langle \sin i \rangle = 4/\pi \simeq 1.27$, assuming random orientation of planetary orbital planes. The other panels are theoretical predictions with $M_* = 0.8\text{--}1.25M_\odot$ for various values of C_1 . The dashed lines express observational limit with radial-velocity measurement precision of $v_r = 10\text{m/s}$. In these models, the magnitude of the metallicity $[\text{Fe}/\text{H}] = 0.1$.

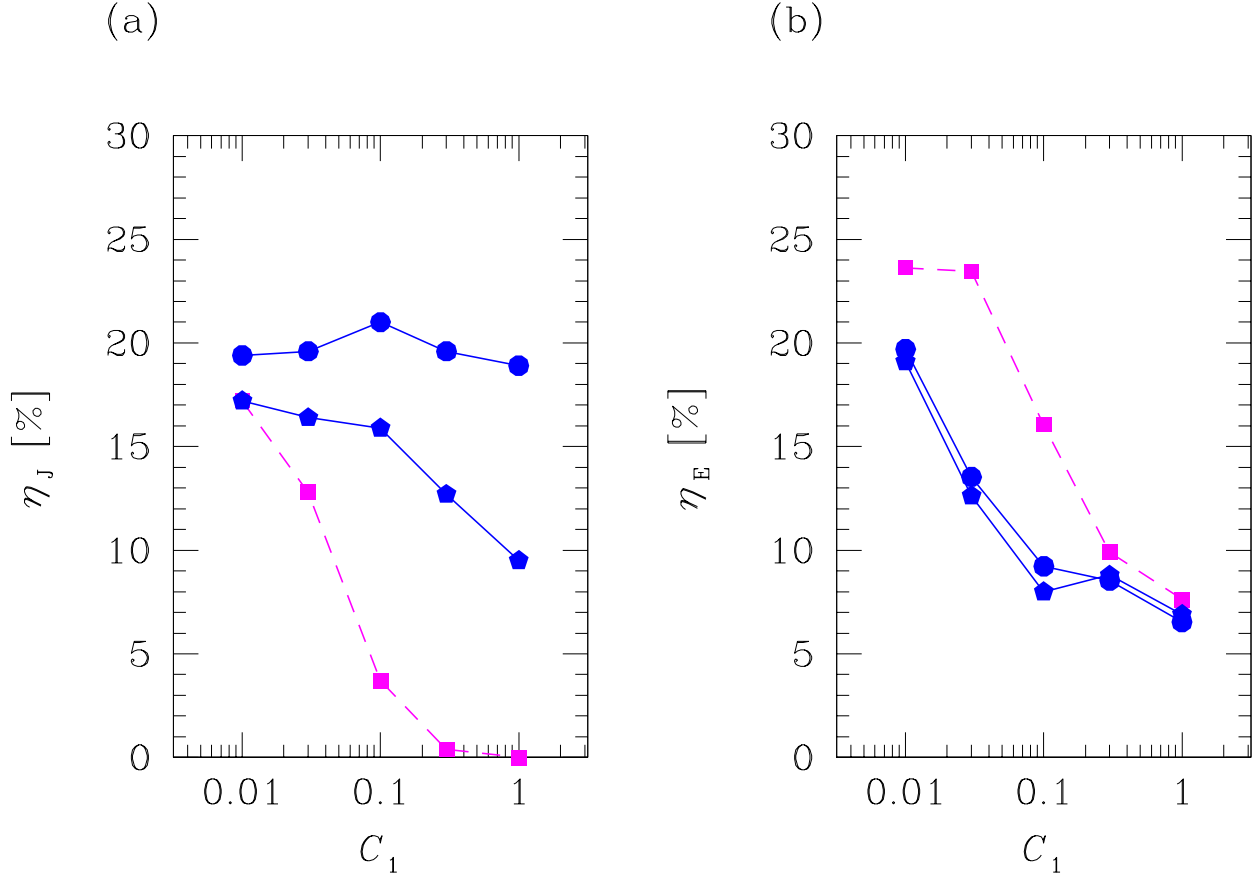


Fig. 4.— The theoretically predicted (a) η_J and (b) η_E (η_\oplus) as functions of the type I migration strength C_1 . η_J is the fraction of stars harboring the planets within the detectability limit of by the magnitude of radial velocity ($v_r > 10\text{m/s}$) and orbital periods ($T_K < 4$ years). η_E (η_\oplus) is the fraction of stars harboring “habitable” planets with $M_p \simeq 0.3 - 10M_\oplus$ and $a \simeq 0.75 - 1.8$ AU around G dwarfs. Filled squares with dashed line, pentagons with solid line, and circles with solid line express the values for the distributions of Figures 3a, b and c, respectively. (The results for $C_1 = 0.01$ are also included.)

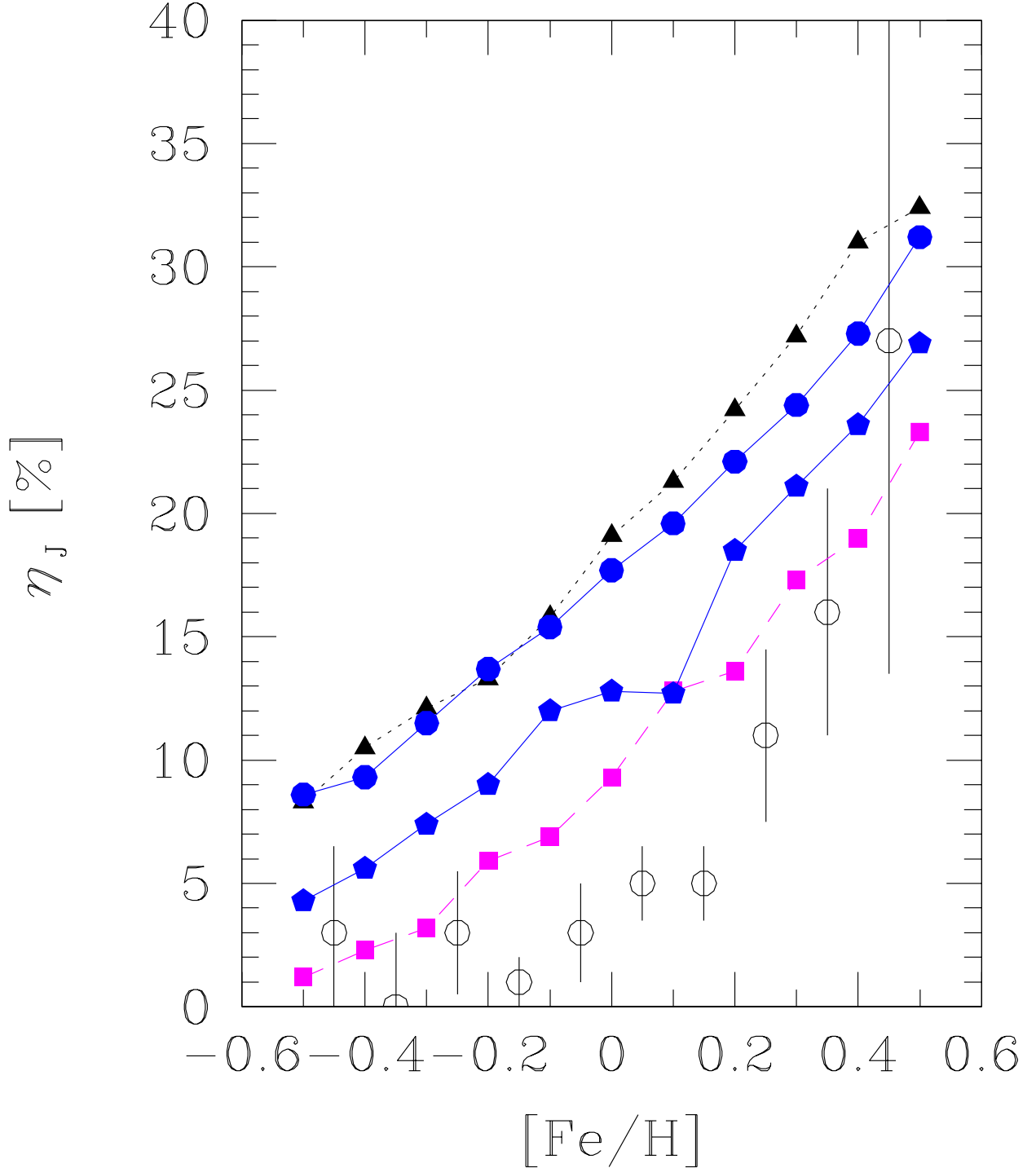


Fig. 5.— Metallicity dependence of η_J . Open circles are observational data by Fischer & Valenti (2005), in which bars express statistical errors. The others are theoretical predictions. Filled triangles with dotted line and squares with dashed line express the results without the Σ_g bump near the ice line. The former and latter are the cases with $C_1 = 0$ and 0.03, respectively. Filled pentagons and circles with solid line express the results with the Σ_g bump. The former and latter are the cases without and with the Σ_d enhancement, in which $C_1 = 0.3$ is used.

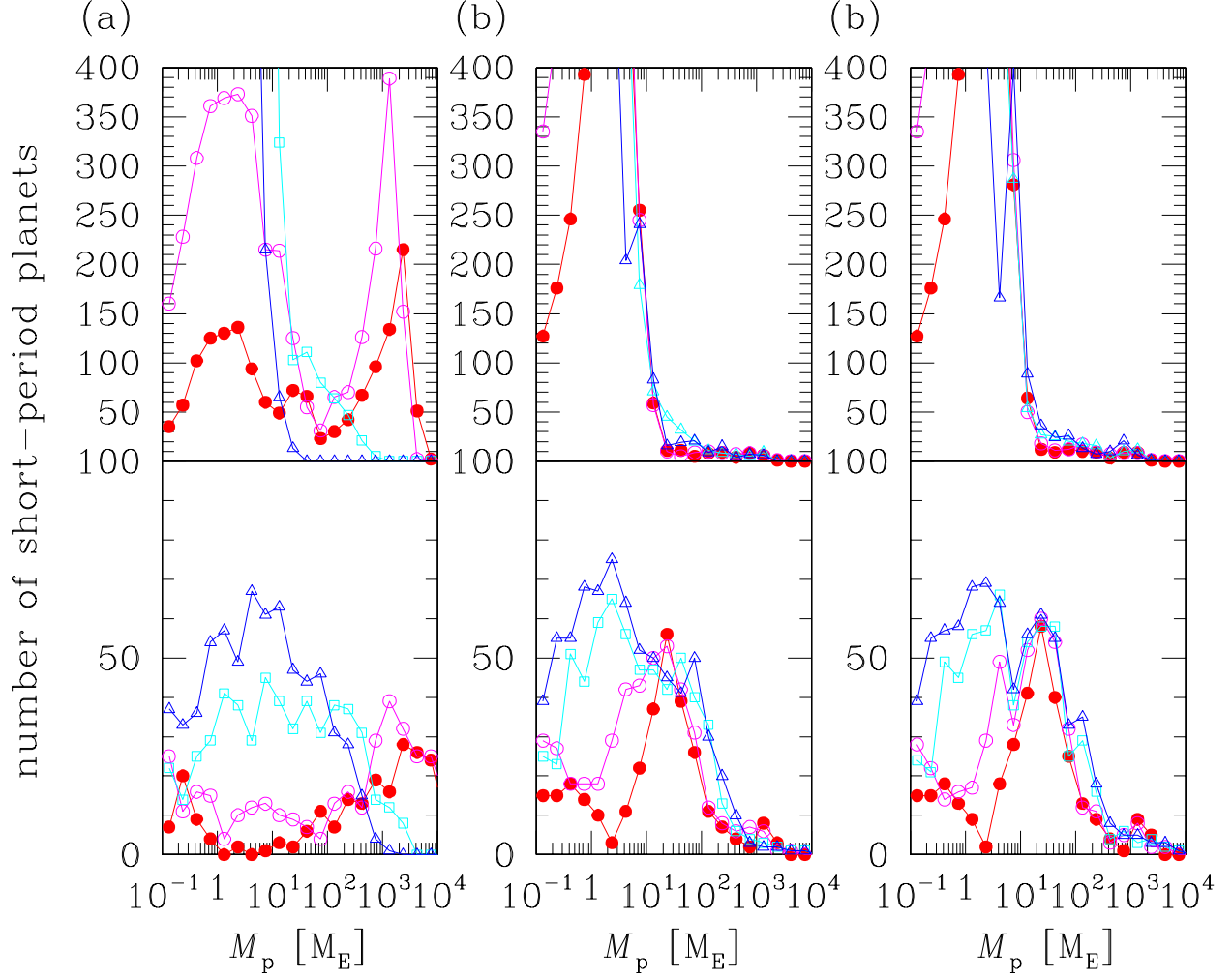


Fig. 6.— Mass functions of short-period planets in the cases (a) without the ice-line barrier, (b) with the ice-line barrier and no Σ_d enhancement, and (c) with the ice-line barrier and the Σ_d enhancement, which are calculated from the distributions of Figures 3a, b and c, respectively. The filled circles, open circles, squares, and triangles express the results for $C_1 = 0.001, 0.01, 0.1$ and 1 . In the upper panels, it is assumed that all the short-period planets survive without any further coagulation. In the lower panels, it is assumed that all the short-period planets in the same disk coagulate into one body.

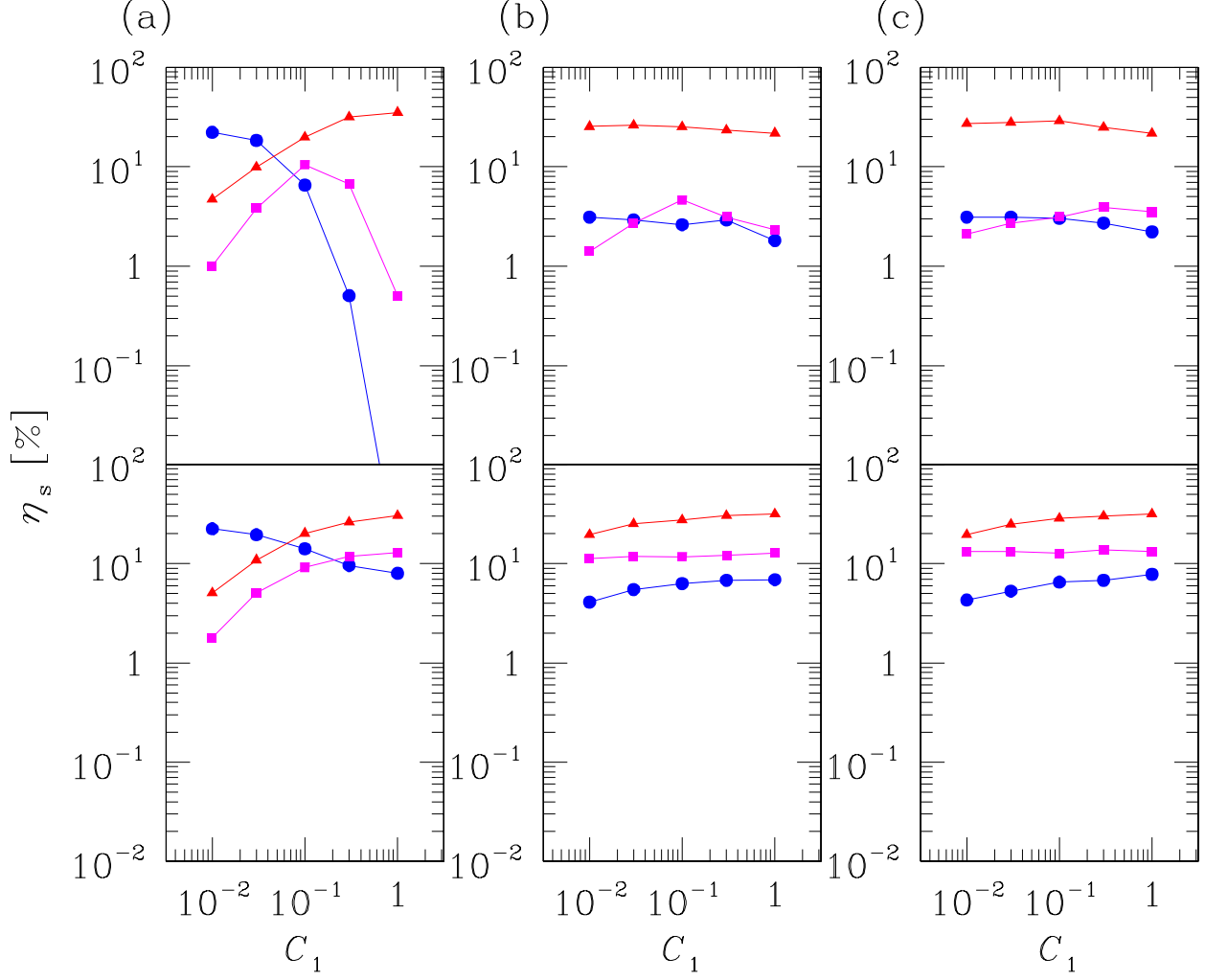


Fig. 7.— Population of giant ($> 100M_{\oplus}$), intermediate-mass ($20 - 100M_{\oplus}$), and lower-mass ($1 - 20M_{\oplus}$) planets as functions of C_1 . They are expressed by circles, squares and triangles, respectively. The meanings of (a), (b) and (c) are the same as those in Figures 6.